OL Organic Letters

pubs.acs.org/OrgLett Letter

Synthesis of Azuleno[1,2,3-*cd*]phenalene and Its π-Extended Buckybowl Derivative

Published as part of Organic Letters special issue "π-Conjugated Molecules and Materials".

Jian Sun, Ziqi Deng, Shuhai Qiu,* Tengteng Chen, David Lee Phillips, and Junzhi Liu*

Cite This: *Org. Lett.* 2025, 27, 8718–8723 Read Online

ACCESS | Metrics & More | Article Recommendations | Supporting Information

ABSTRACT: Azulene-fused molecular carbons have sparked intense research interest in recent years. Herein, we report a facile three-step synthesis of azuleno[1,2,3-*cd*]phenalene (AzPn), a fused system combining azulene and phenalene units, achieving an overall yield of 39.7%. Furthermore, π-extended buckybowl derivatives (**7** and **8**) were synthesized through efficient intramolecular C−H arylation. X-ray analysis confirmed the structures of all three molecular carbons, revealing that the buckybowl derivative adopts a bowl-shaped geometry with a depth of 0.63 Å. Femtosecond transient absorption spectroscopy confirms the formation of triplet species via intersystem crossing in all three molecules following photoexcitation. These molecular carbons exhibit intriguing electronic properties with narrow energy gaps, positioning them as potential building blocks for functional molecular carbons.

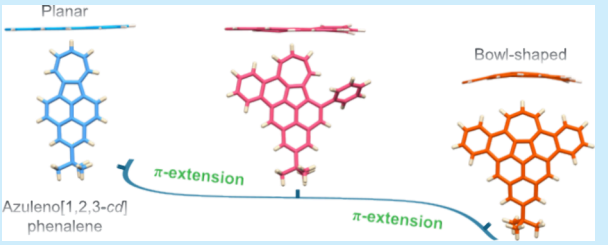

Downloaded via HONG KONG UNIV SCIENCE TECHLGY on January 12, 2026 at 01:18:38 (UTC).
See https://pubs.acs.org/sharingguidelines for options on how to legitimately share published articles.

Non-alternant topological distortion in molecular carbons significantly modifies their optical and electronic properties,[1] thus graphene nanostructures incorporating pentagons and heptagons[2−7] have received considerable attention in recent years owing to their unique photophysical characteristics[8−10] and supramolecular assembly behaviors.[11−15] Azulene, a prominent non-alternant unit featuring a pentagon−heptagon pair, possesses a substantial dipole moment (1.08 D) and distinctive anti-Kasha properties, making it widely employed in molecular carbon engineering.[16−21] Incorporating an azulene unit imparts significant promise to these molecular carbons for applications including single-molecular devices,[22] energy application,[23] organic field-effect transistor (OFETs), spin electronic devices,[24] etc.

Azuleno[1,2,3-*cd*]phenalene (AzPn), a fusion of azulene and phenalene units, is one of the most interesting polycyclic aromatic compounds studied in the early stage. Theoretical studies established its intriguing electronic structure, aromaticity, and magnetic properties.[25−27] In 1975, Hara and Murata[28] first synthesized AzPn (Scheme 1a) to make the theoretical results more reliable; however, the synthetic routine toward AzPn was tedious even with toxic reagents, such as zinc amalgam. Four years later, the synthetic route was further optimized by Murata (Scheme 1b),[29] allowing for a streamlined process with only four steps from azulene. Despite the continued synthetic efforts toward AzPn, its π-extended derivatives have remained unexplored for decades due to difficulties in achieving additional functionalization.

Buckybowl-shaped molecular carbons[30,31] have been extensively studied over the past two decades. However, their synthesis primarily relies on the incorporation of pentagons, which invariably induces positive curvature. In contrast, the integration of a heptagon or azulene unit into bowl-shaped molecular carbons remains elusive. In this work, we achieved the synthesis of AzPn in satisfactory yields through facile and efficient methodologies (Scheme 1c). The introduction of substituted aryl groups at the terminus of triple bonds enables expansion of the AzPn skeleton, affording the π-extended buckybowl derivatives via metal-catalyzed intramolecular arylation. All three compounds are confirmed using single-crystal analysis, revealing configurations ranging from planar to bowl shapes. Furthermore, the energy gaps decreased dramatically with the extension of π conjugation. In addition, a longer structural relaxation time was observed in bowl-shaped **8** due to slow intersystem crossing. These properties suggest potential applications in organic electronics.

The facile synthesis of AzPn in this work is shown as Scheme 1c, and the synthesis of **2** and **3** was in line with our previous work.[32] A selective Sonagashira reaction of **1** with ethynyltrimethylsilane gave **2** in a high yield of 86%. Then, the key azulene units were introduced by the Suzuki reaction of **2** with azuleneboronic acid pinacol ester, affording **3** in an isolated

Received: June 27, 2025
Revised: July 19, 2025
Accepted: July 23, 2025
Published: July 26, 2025

© 2025 American Chemical Society

https://doi.org/10.1021/acs.orglett.5c02662
Org. Lett. 2025, 27, 8718−8723

Scheme 1. (a and b) Synthesis of AzPn in the Early Stage and (c) Synthetic Route of AzPn in This Work

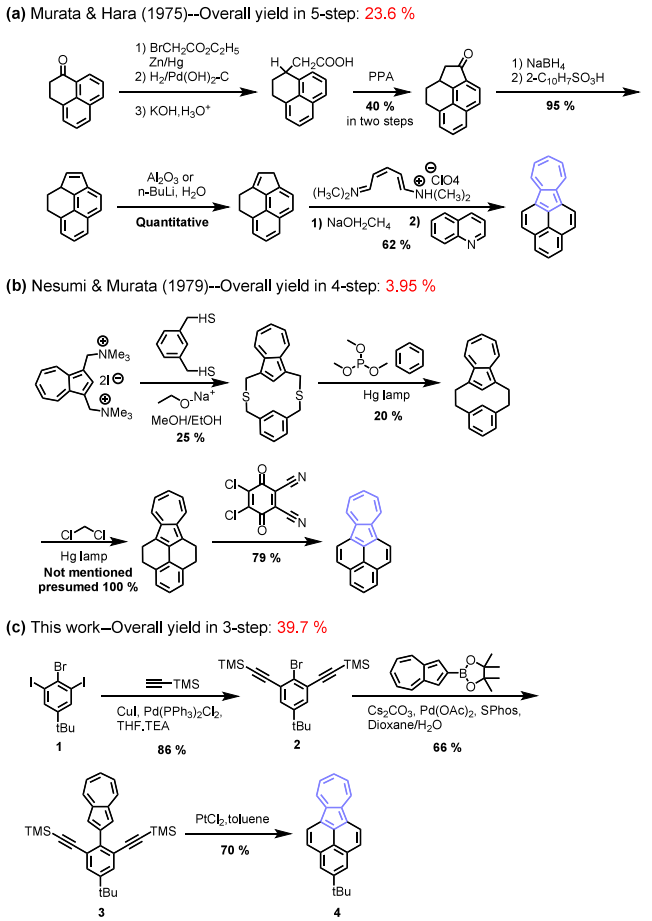

yield of 66%. Finally, compound **4** (^{t}Bu-substituted AzPn) was achieved effectively by platinum (Pt)-catalyzed intramolecular cyclization at the pentagonal ring of azulene.[33−36] Notably, compared to previously reported synthetic approaches (Scheme 1a and b), the synthesis is efficient with only three steps to construct the AzPn skeleton with an overall yield as high as 39.7%. More importantly, the presence of a trimethylsilyl group facilitates further functionalization toward the constructions of π-extended derivatives of AzPn. As shown in Scheme 2, the deprotection of compound **3** went smoothly, followed by a selective Sonagashira reaction with 1-bromo-2-iodobenzene, giving compound **5** in a yield of 87%. Afterward, precursor **6** was obtained by Pt-mediated cyclization in a moderate yield of 53%. Finally, the intramolecular C−H arylation with nickel catalysts yielded both one-side fused compound **7** and two-side fused compound **8** (Scheme 2) in 49 and 24% yields, respectively.

Scheme 2. π-Extension of AzPn-Based Buckybowl Derivatives

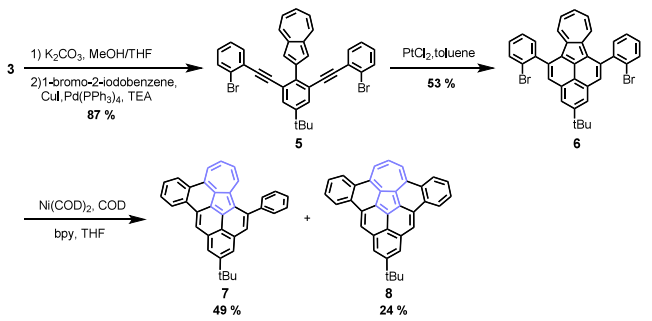

Accordingly, single-crystal X-ray diffraction (SC-XRD) analysis reveals the structural skeletons of those three molecular carbons (Figure 1 and Figures S16−S18). It is

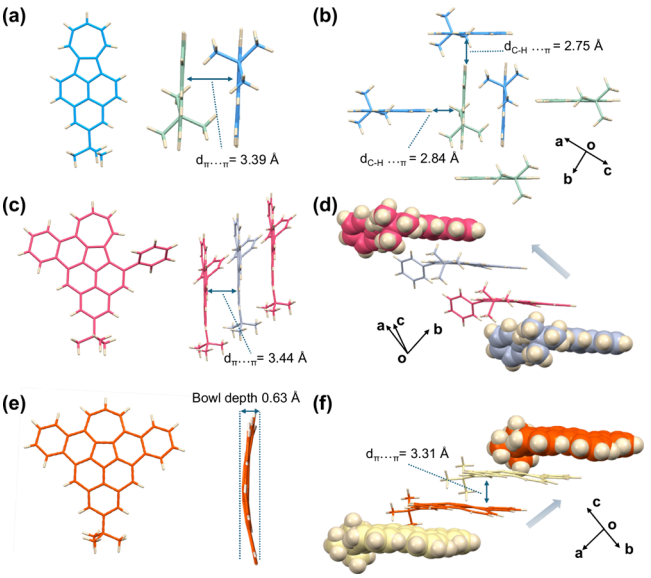

Figure 1. Single-crystal analysis. (a) Front and side views of **4**. (b) Crystal packing of **4**. (c) Front view and side view of **7**. (d) Crystal packing of **7**. (e) Front view and side view (the *tert*-butyl group was omitted) of **8**. (f) Crystal packing of **8**.

noted that compound AzPn was first characterized with the crystal structure, which displays a fully planar skeleton containing one azulene unit in the center. By virtue of sufficient π surfaces, antiparallel dimeric packing with a $\pi\cdots\pi$ distance of 3.39 Å can be observed in the crystal (Figure 1a). Furthermore, all dimers interact through weak C−H$\cdots\pi$ interactions with the distances of 2.75 and 2.84 Å (Figure 1b). When only one additional hexagon was formed during intramolecular annulation, compound **7** remains a planar geometry, as observed in the AzPn skeleton (Figure 1c). The planar conformation tended to stack closely in the solid state, and the intramolecular distance was measured to be as short as 3.44 Å. However, the free rotation of the additional unfused benzene ring resulted in oblique packing with intramolecular $\pi-\pi$ overlap instead of perfect lamellar stacking (Figure 1d). With the incorporation of one more hexagon, the fully fused molecule **8** displayed bowl-shaped conformation with a bowl depth of 0.63 Å (Figure 1e), which was shallower than corannulene.[37] Similar to molecule **7**, the oblique packing was formed by intramolecular $\pi-\pi$ interactions with 3.31 Å, and the $\pi\cdots\pi$ overlap could also be observed in the crystalline lattice (Figure 1f).

The well-resolved UV−vis absorption spectra of three molecules were measured in a dichloromethane (DCM) solution, as shown in Figure 2a. Due to the relatively topological molecular skeleton, all three molecules displayed comparable absorption spectra. For molecule **4**, the absorption band was located lower than 500 nm, indicating the optical energy gap of 2.48 eV. Moreover, with the increasing π conjugation, the absorption edge of molecule **7** extended to

https://doi.org/10.1021/acs.orglett.5c02662
Org. Lett. 2025, 27, 8718−8723

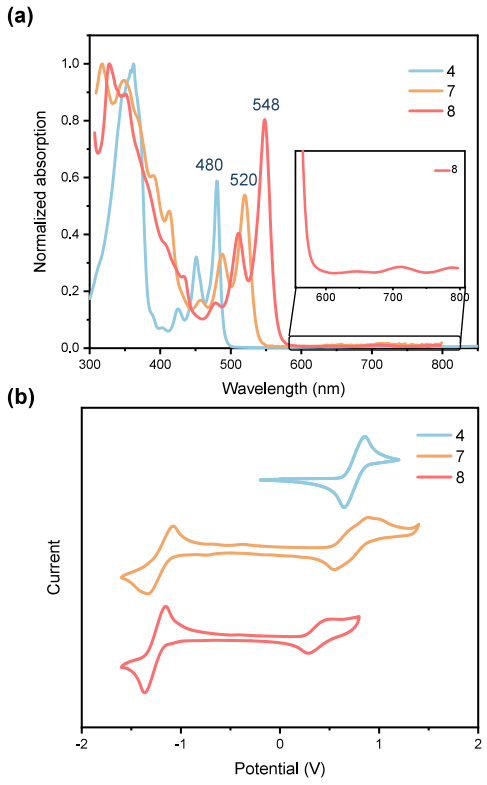

Figure 2. (a) Normalized UV−vis absorption spectra of compounds **4**, **7**, and **8** in DCM (10^{-5} M) (Inset) Zoom in absorption of **8** in the range of 600−800 nm. (b) Cyclic voltammograms (IUPAC convention) of compounds **4**, **7**, and **8** measured on the silver reference electrode, glassy carbon working electrode, and platinum wire counter electrode in degassed DCM solution containing 0.1 M *n*-Bu_4NPF_6 and 2 mM sample at room temperature. It was recorded starting at 0.00 V vs ferrocene/ferrocenium (Fc/Fc^+) and scanned in the positive direction at a rate of 50 mV/s.

550 nm and the onset absorption of molecule **8** was measured as 585 nm by fusing more aromatic rings. In addition, a low-intensity absorption tail was observed for **8** between 600 and 800 nm. Theoretical calculations (Figure S20) assign these low-energy absorptions to HOMO → LUMO + 1 transitions with a low oscillator strength. Accordingly, the optical energy gaps of **7** and **8** were calculated to be 2.25 and 2.12 eV, respectively. To understand the electrochemical behaviors of this series of molecules, cyclic voltammetry was conducted in anhydrous DCM (Figure 2b), and electrochemical data are provided in Table 1. Compound **4** displayed one reversible oxidation with half-wave potential at 0.65 eV, indicating the low highest occupied molecular orbital (HOMO) level of −5.05 eV. However, both compounds **7** and **8** exhibited the reversible oxidation and reduction with half-wave potentials at 0.52 and 0.23 V and −1.05 and −1.13 V, respectively. In addition, compound **7** exhibited another two oxidation waves,

Table 1. Summary of the Electrochemical Properties of Molecules 4, 7, and 8

name	$E_{ox.1}$[a] (V)	$E_{red.1}$[a] (V)	E_{HOMO} (eV)	E_{LUMO} (eV)	ΔE_{gap} (eV)
4	0.65		−5.05		
7	0.52	−1.05	−4.92	−3.35	1.57
8	0.23	−1.13	−4.63	−3.27	1.36

[a]Redox potentials were measured as half-wave potentials.

at 0.75 and 0.95. Thus, the corresponding energy gaps of **7** and **8** were determined as 1.57 and 1.36 eV (Table 1), which are significantly smaller than those typically observed in all-carbon buckybowls.[6,38,39]

The geometries of all three molecules were optimized by utilizing density functional theory (DFT) calculations at the B3LYP level with the 6-31G(d) basis set (Figure 3a).

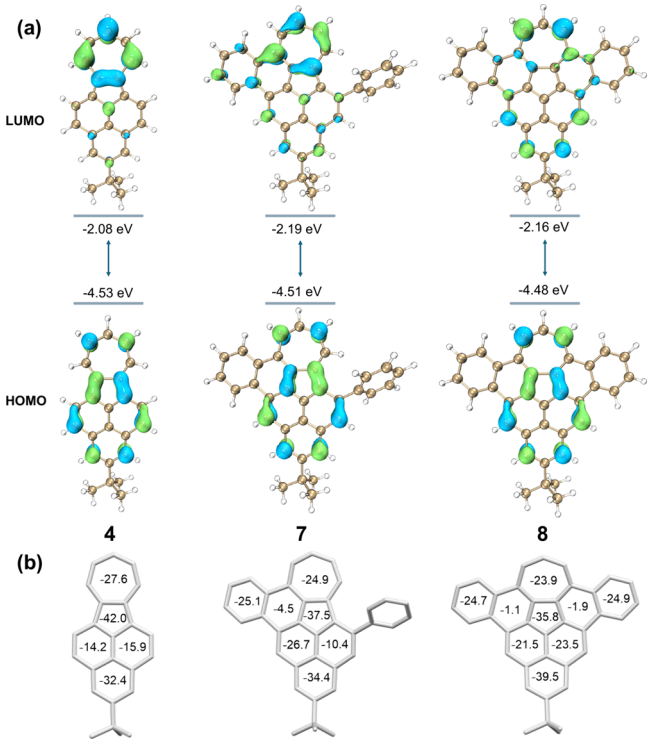

Figure 3. (a) Optimized frontier molecular orbitals of molecules **4** (left), **7** (middle), and **8** (right) calculated at the B3LYP/6-31G(d) level (isovalue = 0.05). (b) Calculated NICS $(1)_{zz\text{-}avg}$ values of molecules **4** (left), **7** (middle), and **8** (right).

According to the calculation results,[40] the HOMO energy levels increased with the conjugation expansion and the LUMO energy levels of molecules **7** and **8** were slightly higher than that of **4**. All three molecules displayed a similar HOMO electron distribution on the central AzPn core, and the LUMO electron was mainly located at heptagons; however, for **8**, the LUMO tended to delocalize on the AzPn core. To further explore the aromaticity of the series of AzPn derivatives, nuclear-independent chemical shift (NICS) calculation (Figure 3b) was conducted and the fused rings of these three compounds exhibited negative values, suggesting their global aromatic properties. For the newly formed hexagonal rings, the NICS values for **7** and **8** were −4.5, −1.1, and −1.9, respectively, indicating their weak aromatic or non-aromatic characteristics. Additionally, the calculated ACID plots (Figure S19) also indicated their global aromaticity, which is in accordance with NICS calculations.

To further elucidate how π extension influences the excited-state behavior of these molecular carbons, the deactivation pathways and photodynamics of molecules **4**, **7**, and **8** were investigated using femtosecond transient absorption (fs-TA) spectroscopy with 360 nm excitation. As shown in Figure 4, these compounds showed similar wavy features within the early 100 ps, which resulted from the overlap between the

https://doi.org/10.1021/acs.orglett.5c02662
Org. Lett. 2025, 27, 8718−8723

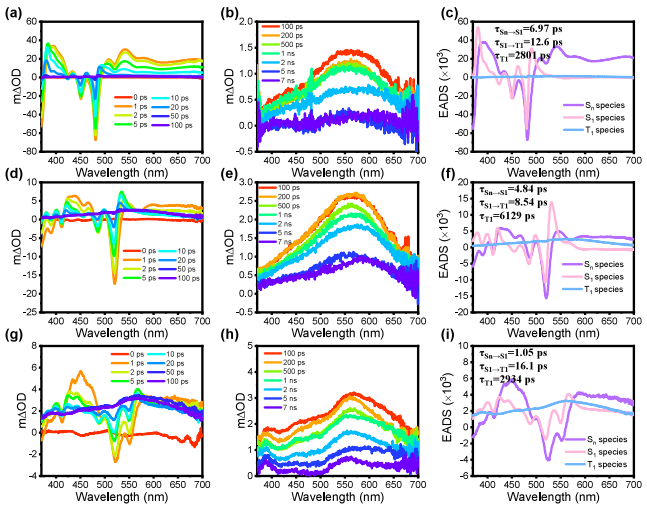

Figure 4. (a) Fs-TA spectra from 0 to 100 ps, (b) fs-TA spectra from 100 ps to 7 ns, and (c) EADS species obtained from the global analysis of **4** in toluene solution in air. (d) Fs-TA spectra from 0 to 100 ps, (e) fs-TA spectra from 100ps to 7 ns, and (f) EADS species obtained from the global analysis of **7** in toluene solution in air. (g) Fs-TA spectra from 0 to 100 ps, (h) fs-TA spectra from 100 ps to 7 ns, and (i) EADS species obtained from the global analysis of **8** in toluene solution in air.

excited-state absorption (ESA) and ground-state blenching (GSB) signal. Subsequently, the signal will sharply decrease and remain a broad band centered at around 560 nm. Global analysis based on the sequential model was carried out, and three evolution-associated difference spectra (EADS) species were obtained from the fs-TA contour plot of these molecules. As a result, the first species show an obvious feature at 600−700 nm, which will disappear in the EADS of the second species. Considering that the molecules were excited to a higher excited state, this species could be assigned to S_n state species, and it will decay to the lowest singlet S_1 state (the second EADS species) by internal conversion (IC). The third species showed a much longer lifetime than the S_n and S_1 states, which was proven to be the triplet species (Figure S22). The fs-TA spectra of three compounds were measured under a N_2 atmosphere, and the lifetimes of the first two species exhibit very close values compared to the molecules measured in air, while the third lifetime was much longer in the N_2 atmosphere (Figure S21). Interestingly, compound **7** exhibited the highest intersystem crossing (ISC) rate, followed by **4** and then **8**. To understand this trend, we investigated the singlet−triplet energy gap and spin−orbit coupling matrix elements (SOCME) using TD-DFT calculations (Figure S23). The calculations show that the S_1 state of all three molecules can undergo transitions to the T_1 and T_2 states. Molecule **7** possesses the largest SOCME for these transitions ($S_1 \rightarrow T_1$, 0.04 cm^{-1}; $S_1 \rightarrow T_2$, 0.01 cm^{-1}). In contrast, molecule **4** has a larger ΔE_{ST} and smaller SOCME than that of **7**, resulting in a lower ISC rate. Compound **8** exhibits the smallest SOCME (<0.005 cm^{-1}), explaining its slowest ISC process.

In summary, we reported an efficient synthesis of AzPn featuring a streamlined three-step route with an impressive overall yield of 39.7%. The structural skeleton of AzPn was validated by X-ray single-crystal analysis. Furthermore, we pioneered the exploration of π-extended AzPn derivatives through intramolecular C−H arylation, affording novel buckybowls containing one azulene unit. Electrochemical studies revealed distinct reversible redox behaviors for molecules **7** and **8**, while only a reversible oxidation wave was detected for **4**. Fs-TA spectroscopy confirmed the involvement of ISC in the excited-state deactivation pathway. Theoretical calculations further identified the key factors governing ISC rates across these three molecules. Moreover, these AzPn-based derivatives possess narrow energy gaps, highlighting their potential as novel building blocks for constructing low-band gap molecular carbon materials.

■ ASSOCIATED CONTENT

Data Availability Statement

The data underlying this study are available in the published article and its Supporting Information.

Supporting Information

The Supporting Information is available free of charge at https://pubs.acs.org/doi/10.1021/acs.orglett.5c02662.

Details of synthetic methods, NMR spectra, high-resolution MS, X-ray single-crystal data, and DFT calculations (PDF)

Accession Codes

Deposition Numbers 2362129, 2362132, and 2428001 contain the supplementary crystallographic data for this paper. These data can be obtained free of charge via the joint Cambridge Crystallographic Data Centre (CCDC) and Fachinformations-zentrum Karlsruhe Access Structures service.

■ AUTHOR INFORMATION

Corresponding Authors

Shuhai Qiu − *Department of Chemistry, The University of Hong Kong, Hong Kong, China*; Email: qiush@hku.hk

Junzhi Liu − *Department of Chemistry, The University of Hong Kong, Hong Kong, China; State Key Laboratory of Synthetic Chemistry, HKU-CAS Joint Laboratory on New Materials and Shanghai-Hong Kong Joint Laboratory on Chemical Synthesis, The University of Hong Kong, Hong Kong, China; Materials Innovation Institute for Life Sciences and Energy (MILES), HKU-SIRI, Shenzhen 518000, China*; orcid.org/0000-0001-7146-0942; Email: juliu@hku.hk

Authors

Jian Sun − *Department of Chemistry, The University of Hong Kong, Hong Kong, China*

Ziqi Deng − *Department of Chemistry, The Hong Kong University of Science and Technology, Hong Kong, China*

Tengteng Chen − *Department of Chemistry, The Hong Kong University of Science and Technology, Hong Kong, China*

David Lee Phillips − *Department of Chemistry, The University of Hong Kong, Hong Kong, China*; orcid.org/0000-0002-8606-8780

Complete contact information is available at: https://pubs.acs.org/10.1021/acs.orglett.5c02662

Author Contributions

J.S. and J.L. designed the project. J.S. synthesized all the compounds and did the characterization. Z.D., T.C., and D.L.P. designed and performed the transient absorption analysis. The manuscript was written by J.S. and revised through contributions of S.Q. and J.L.

https://doi.org/10.1021/acs.orglett.5c02662
Org. Lett. 2025, 27, 8718−8723

Notes

The authors declare no competing financial interest.

■ ACKNOWLEDGMENTS

This work was supported by the Hong Kong Research Grants Council (27301720, 17304021, and 17309023) and the National Natural Science Foundation of China (22122114). J.L. is grateful for the funding from The University of Hong Kong (HKU) and ITC to the SKL. The authors thank the UGC funding administered by HKU for supporting the Time-of-Flight Mass Spectrometry Facilities under the Support for Interdisciplinary Research in Chemical Science. The authors acknowledge the computer cluster (HPC2021) of HKU for generous allocations of computer resources. The work described in this paper was partially supported by a grant from the Co-funding Mechanism on Joint Laboratories with the Chinese Academy of Sciences (CAS) sponsored by the Research Grants Council of the Hong Kong Special Administrative Region, China, and the CAS (Projects JLFS/P-701/24 and JLFS/P-404/24).

■ REFERENCES

(1) Wang, X.-Y.; Yao, X.; Müllen, K. Polycyclic aromatic hydrocarbons in the graphene era. *Sci. China Chem.* **2019**, *62*, 1099−1144.
(2) Chaolumen; Stepek, I. A.; Yamada, K. E.; Ito, H.; Itami, K. Construction of Heptagon-Containing Molecular Nanocarbons. *Angew. Chem., Int. Ed.* **2021**, *60*, 23508−23532.
(3) Konishi, A.; Yasuda, M. Breathing New Life into Nonalternant Hydrocarbon Chemistry: Syntheses and Properties of Polycyclic Hydrocarbons Containing Azulene, Pentalene, and Heptalene Frameworks. *Chem. Lett.* **2021**, *50*, 195−212.
(4) Kawasumi, K.; Zhang, Q.; Segawa, Y.; Scott, L. T.; Itami, K. A grossly warped nanographene and the consequences of multiple odd-membered-ring defects. *Nat. Chem.* **2013**, *5*, 739−744.
(5) Liang, Y.; Wang, S.; Tang, M.; Wu, L.; Bian, L.; Jiang, L.; Tang, Z.-B.; Liu, J.; Guan, A.; Liu, Z. Cascade Synthesis of Benzotriazulene with Three Embedded Azulene Units and Large Stokes Shifts. *Angew. Chem., Int. Ed.* **2023**, *62*, No. e202218839.
(6) Ogawa, N.; Yamaoka, Y.; Takikawa, H.; Yamada, K.-i.; Takasu, K. Helical Nanographenes Embedded with Contiguous Azulene Units. *J. Am. Chem. Soc.* **2020**, *142*, 13322−13327.
(7) Han, Y.; Xue, Z.; Li, G.; Gu, Y.; Ni, Y.; Dong, S.; Chi, C. Formation of Azulene-Embedded Nanographene: Naphthalene to Azulene Rearrangement During the Scholl Reaction. *Angew. Chem., Int. Ed.* **2020**, *59*, 9026−9031.
(8) Pigulski, B.; Shoyama, K.; Würthner, F. NIR-Absorbing π-Extended Azulene: Non-Alternant Isomer of Terrylene Bisimide. *Angew. Chem., Int. Ed.* **2020**, *59*, 15908−15912.
(9) Luo, H.; Liu, J. Facile Synthesis of Nitrogen-Doped Nanographenes with Joined Nonhexagons via a Ring Expansion Strategy. *Angew. Chem., Int. Ed.* **2023**, *62*, No. e202302761.
(10) Reale, M.; Sciortino, A.; Cruz, C. M.; Cannas, M.; Maçoas, E.; Campaña, A. G.; Messina, F. The photophysics of distorted nanographenes: Ultra-slow relaxation dynamics, memory effects, and delayed fluorescence. *Carbon* **2023**, *206*, 45−52.
(11) Zank, S.; Fernández-García, J. M.; Stasyuk, A. J.; Voityuk, A. A.; Krug, M.; Solà, M.; Guldi, D. M.; Martín, N. Initiating Electron Transfer in Doubly Curved Nanographene Upon Supramolecular Complexation of C_{60}. *Angew. Chem., Int. Ed.* **2022**, *61*, No. e202112834.
(12) Zhou, Z.; Zhu, Y.; Fernández-García, J. M.; Wei, Z.; Fernández, I.; Petrukhina, M. A.; Martín, N. Stepwise reduction of a corannulene-based helical molecular nanographene with Na metal. *Chem. Commun.* **2022**, *58*, 5574−5577.
(13) Fernández-García, J. M.; Evans, P. J.; Medina Rivero, S.; Fernández, I.; García-Fresnadillo, D.; Perles, J.; Casado, J.; Martín, N. π-Extended Corannulene-Based Nanographenes: Selective Formation of Negative Curvature. *J. Am. Chem. Soc.* **2018**, *140*, 17188−17196.
(14) Jiménez, V. G.; David, A. H. G.; Cuerva, J. M.; Blanco, V.; Campaña, A. G. A Macrocycle Based on a Heptagon-Containing Hexa-peri-hexabenzocoronene. *Angew. Chem., Int. Ed.* **2020**, *59*, 15124−15128.
(15) Kato, K.; Takaba, K.; Maki-Yonekura, S.; Mitoma, N.; Nakanishi, Y.; Nishihara, T.; Hatakeyama, T.; Kawada, T.; Hijikata, Y.; Pirillo, J.; Scott, L. T.; Yonekura, K.; Segawa, Y.; Itami, K. Double-Helix Supramolecular Nanofibers Assembled from Negatively Curved Nanographenes. *J. Am. Chem. Soc.* **2021**, *143*, 5465−5469.
(16) Xin, H.; Hou, B.; Gao, X. Azulene-based π-functional materials: design, synthesis, and applications. *Acc. Chem. Res.* **2021**, *54*, 1737−1753.
(17) Xin, H.; Gao, X. Application of azulene in constructing organic optoelectronic materials: New tricks for an old dog. *ChemPlusChem* **2017**, *82*, 945−956.
(18) Duan, C.; Xin, H.; Gao, X. Recent progress in chemistry of non-benzenoid carbohelicenes. *Tetrahedron Lett.* **2023**, *123*, 154553.
(19) Fei, Y.; Liu, J. Synthesis of defective nanographenes containing joined pentagons and heptagons. *Adv. Sci.* **2022**, *9*, 2201000.
(20) Luo, H.; Liu, J. Non-Alternant Nanographenes Bearing N-Doped Non-Hexagonal Pairs: Synthesis, Structural Analysis and Photophysical Properties. *Angew. Chem., Int. Ed.* **2024**, *63*, No. e202410759.
(21) Pigulski, B. Recent advances and future challenges in the bottom-up synthesis of azulene-embedded nanographenes. *Beilstein J. Org. Chem.* **2025**, *21*, 1272−1305.
(22) Zhang, C.; Kong, Y.; Xiang, J.; Chen, S.; Kornyshev, A. A.; Ulstrup, J.; Gao, X.; Zhang, G.; Li, Y.; Li, J. Switchable modes of azulene-based single molecule-electrode coupling controlled by interfacial charge distribution. *Chem. Sci.* **2025**, *16*, 1353−1363.
(23) Huang, J.; Huang, S.; Zhao, Y.; Feng, B.; Jiang, K.; Sun, S.; Ke, C.; Kymakis, E.; Zhuang, X. Azulene-Based Molecules, Polymers, and Frameworks for Optoelectronic and Energy Applications. *Small Methods* **2020**, *4*, 2000628.
(24) Song, Y.; Su, Y.; Zhao, P.; Zhang, G.-P.; Wang, C.-K.; Chen, G. Azulene-like molecular devices with high spin filtering, strong spin rectifying, and giant magnetoresistance effects. *Org. Electron.* **2018**, *59*, 113−120.
(25) Koyanagi, T.; Shin, Y.; Yamaguchi, H. Electronic Structures and Spectra of Azulenophenalenes. *Bull. Chem. Soc. Jpn.* **1977**, *50*, 345−348.
(26) Tajiri, A.; Hatano, M.; Murata, I.; Nakasuji, K. the Magnetic Circular Dichroism Spectrum of Azulenod[1,2,3-*cd*]phenalene. *Chem. Lett.* **1976**, *5*, 543−546.
(27) Gleiter, R.; Spanget-Larsen, J.; Thulstrup, E. W.; Murata, I.; Nakasuji, K.; Jutz, C. The Electronic Structure of Azuleno[1,2,3-*cd*]phenalene and Azuleno[5,6,7-*cd*]phenalene, a Comparison. *Helv. Chim. Acta* **1976**, *59*, 1459−1468.
(28) Murata, I.; Nakasuji, K.; Yamamoto, K.; Nakazawa, T.; Kayane, Y.; Kimura, A.; Hara, O. Synthesis and Properties of Azuleno[1,2,3-*cd*]phenalene. *Angew. Chem., Int. Ed.* **1975**, *14*, 170−171.
(29) Nesumi, Y.; Nakazawa, T.; Murata, I. Synthesis of [2.2]-Metacyclo(1,3)azulenophane and Its Conversion to Azuleno[1,2,3-*cd*]phenalene. *Chem. Lett.* **1979**, *8*, 771−774.
(30) Chen, Y.; Zhang, L. Buckybowl-Based Nanocarbons: Synthesis, Properties, and Applications. *Acc. Chem. Res.* **2025**, *58*, 762−776.
(31) Wu, Y.-T.; Siegel, J. S. Aromatic molecular-bowl hydrocarbons: synthetic derivatives, their structures, and physical properties. *Chem. Rev.* **2006**, *106*, 4843−4867.
(32) Sun, J.; Deng, Z.; Lee Phillips, D.; Liu, J. Exploring diverse supramolecular tessellation through hierarchical assemblies of non-alternant nanographene. *Proc. Natl. Acad. Sci. U.S.A.* **2025**, *122*, No. e2426059122.

https://doi.org/10.1021/acs.orglett.5c02662
Org. Lett. 2025, 27, 8718−8723

(33) Duan, C.; Zhang, J.; Xiang, J.; Yang, X.; Gao, X. Azulene-Embedded [*n*]Helicenes (*n* = 5, 6 and 7). *Angew. Chem., Int. Ed.* **2022**, *61*, No. e202201494.
(34) Guo, J.; Du, F.; Yu, B.; Du, P.; Li, H.; Zhang, J.; Xin, H. Heptacyclic aromatic hydrocarbon isomers with two azulene units fused. *Chem. Sci.* **2024**, *15*, 12589−12597.
(35) Shiotari, A.; Nakae, T.; Iwata, K.; Mori, S.; Okujima, T.; Uno, H.; Sakaguchi, H.; Sugimoto, Y. Strain-induced skeletal rearrangement of a polycyclic aromatic hydrocarbon on a copper surface. *Nat. Commun.* **2017**, *8*, 16089.
(36) Mathey, P.; Fernández, I.; Morin, J.-F. Exploring C−C bond formation reactions for expanding azulene derivatives linked at the 2- and/or 6-positions. *New J. Chem.* **2024**, *48*, 4801−4809.
(37) Rabideau, P. W.; Sygula, A. Buckybowls: polynuclear aromatic hydrocarbons related to the buckminsterfullerene surface. *Acc. Chem. Res.* **1996**, *29*, 235−242.
(38) Wang, J.; Gámez, F. G.; Marín-Beloqui, J.; Diaz-Andres, A.; Miao, X.; Casanova, D.; Casado, J.; Liu, J. Synthesis of a Dicyclohepta[*a*,*g*]heptalene-Containing Polycyclic Conjugated Hydrocarbon and the Impact of Non-Alternant Topologies. *Angew. Chem., Int. Ed.* **2023**, *62*, No. e202217124.
(39) Ong, A.; Tao, T.; Jiang, Q.; Han, Y.; Ou, Y.; Huang, K.-W.; Chi, C. Azulene-Fused Acenes. *Angew. Chem., Int. Ed.* **2022**, *134*, No. e202209286.
(40) Lu, T.; Chen, F. Multiwfn: A multifunctional wavefunction analyzer. *J. Comput. Chem.* **2012**, *33*, 580−592.

https://doi.org/10.1021/acs.orglett.5c02662
Org. Lett. 2025, 27, 8718−8723